Higher-Order Topology, Monopole Nodal Lines, and the Origin of Large Fermi Arcs in Transition Metal Dichalcogenides XTe_2 ($X = Mo, W$)

Zhijun Wang,[1,2,3] Benjamin J. Wieder,[3] Jian Li,[4] Binghai Yan,[5] and B. Andrei Bernevig[3,6,7]
[1]*Beijing National Laboratory for Condensed Matter Physics, and Institute of Physics, Chinese Academy of Sciences, Beijing 100190, China*
[2]*University of Chinese Academy of Sciences, Beijing 100049, China*
[3]*Department of Physics, Princeton University, Princeton, New Jersey 08544, USA*
[4]*School of Science, Westlake University, 18 Shilongshan Road, Hangzhou 310024, China*
[5]*Department of Condensed Matter Physics, Weizmann Institute of Science, Rehovot 7610001, Israel*
[6]*Dahlem Center for Complex Quantum Systems and Fachbereich Physik, Freie Universität Berlin, Arnimallee 14, 14195 Berlin, Germany*
[7]*Max Planck Institute of Microstructure Physics, 06120 Halle, Germany*

(Received 2 July 2018; revised manuscript received 16 September 2019; published 28 October 2019)

In recent years, transition metal dichalcogenides (TMDs) have garnered great interest as topological materials. In particular, monolayers of centrosymmetric β-phase TMDs have been identified as 2D topological insulators (TIs), and bulk crystals of noncentrosymmetric γ-phase $MoTe_2$ and WTe_2 have been identified as type-II Weyl semimetals. However, angle-resolved photoemission spectroscopy and STM probes of these semimetals have revealed huge, arclike surface states that overwhelm, and are sometimes mistaken for, the much smaller topological surface Fermi arcs of bulk type-II Weyl points. In this Letter, we calculate the bulk and surface electronic structure of both β- and γ-$MoTe_2$. We find that β-$MoTe_2$ is, in fact, a $\mathbb{Z}_4$-nontrivial higher-order TI (HOTI) driven by double band inversion and exhibits the same surface features as γ-$MoTe_2$ and γ-WTe_2. We discover that these surface states are not topologically trivial, as previously characterized by the research that differentiated them from the Weyl Fermi arcs but, rather, are the characteristic split and gapped fourfold Dirac surface states of a HOTI. In β-$MoTe_2$, this indicates that it would exhibit helical pairs of hinge states if it were bulk insulating, and in γ-$MoTe_2$ and γ-WTe_2, these surface states represent vestiges of HOTI phases without inversion symmetry that are nearby in parameter space. Using nested Wilson loops and first-principles calculations, we explicitly demonstrate that, when the Weyl points in γ-$MoTe_2$ are annihilated, which may be accomplished by symmetry-preserving strain or lattice distortion, γ-$MoTe_2$ becomes a nonsymmetry-indicated, noncentrosymmetric HOTI. We also show that, when the effects of spin-orbit coupling are neglected, β-$MoTe_2$ is a nodal-line semimetal with $\mathbb{Z}_2$-nontrivial monopole nodal lines (MNLSM). This finding confirms that MNLSMs driven by double band inversion are the weak-spin-orbit coupling limit of HOTIs, implying that MNLSMs are higher-order topological semimetals with flat-band-like hinge states, which we find to originate from the corner modes of 2D "fragile" TIs.

DOI: 10.1103/PhysRevLett.123.186401

Over the past decade, the number of topological insulating and semimetallic phases identified in real materials has grown immensely. With the discovery of increasingly intricate topological insulators (TIs) and semimetals (SMs), such as higher-order TIs (HOTIs) [1–12] and unconventional fermion SMs [13–18], previously overlooked, but readily accessible compounds, including bismuth [19] and chiral B20 [20–24] crystals, have been experimentally verified as topologically nontrivial. In this Letter, we extend the theory and experimental applicability of higher-order topology by recognizing that the XTe_2 ($X = Mo, W$) family [25–30] of transition metal dichalcogenides (TMDs), a large, well-studied, and readily synthesizable class of materials, are HOTIs, and not topologically trivial. XTe_2 TMDs, which exhibit a trivial magnetoelectric polarizability [11,31–38], therefore, provide an intriguing experimental platform for examining topological response effects beyond the magnetoelectric effect [39–43]. We also draw connections between an exotic class of nodal-line SMs (NLSMs) [44–46] and the recently introduced notion of "fragile" topology [11,47–51], leading to the discovery of fractionally charged corner modes in fragile TIs. Our findings further establish the seemingly esoteric concept of higher-order topology as crucial for characterizing topological transport and response effects in everyday materials.

All of the spinful TIs discovered to date represent the gapped, spin-orbit coupled (strong-SOC) limits of gapless topological (SM) phases without SOC. This intrinsic link

between gapped and gapless phases has defined topological condensed matter physics since the recognition that graphene [52–54] and HgTe gap into $\mathbb{Z}_2$ TIs [55,56] under the introduction of SOC [57]. As the number of known topological SMs has increased [13–18,58–70], the number of known topological (crystalline) insulators realized by gapping them has kept pace [7,71–76]. In one particularly simple example, an SM phase with a ring of linearly dispersing degeneracies, known as a "nodal line" (NL), can occur in a weak-SOC crystal with only inversion ($\mathcal{I}$) and time-reversal ($\mathcal{T}$) symmetries [44,77,78]. NLs may be created and annihilated at single, time-reversal-invariant (TRIM) points in the Brillouin zone (BZ) by inverting bands with opposite parity ($\mathcal{I}$) eigenvalues [44], such that the number of NLs is constrained by the same Fu-Kane parity criterion [79,80] that indicates 3D TI phases in strong-SOC crystals. This recognition has driven the rapid identification of candidate NLSMs, including Ca_3P_2 [81], $Cu_3(Pd, Zn)N$ [44,77], and 3D graphene networks [82], all of which exhibit characteristic nearly flat-band "drumhead" surface states. Crucially, it also implies that weak-SOC NLSMs gap directly into 3D TIs upon the introduction of $\mathcal{I}$-symmetric SOC [44].

Very recently, fundamentally distinct $\mathcal{I}$- and $\mathcal{T}$-symmetric SMs and insulators have been proposed that escape this paradigm. In [45], Fang *et al.* introduced a second kind of weak-SOC NL, which, unlike the previous example, can only be removed by pairwise annihilation. Though the mechanisms underpinning the protection and identification of these "monopole-charged" NLs (MNLs) have been explored in detail [46,83,84]; MNLs have, thus far, only been proposed in magnonic systems [85] and 3D graphdiyne [46,86]. Recent works have also identified 3D "higher-order" TIs [1–12] stabilized by only $\mathcal{I}$ and $\mathcal{T}$ symmetries [3,19,87–90]. Notably, 3D HOTIs exhibit gapped 2D surfaces and gapless 1D hinges with characteristic helical modes [2–4], which represent the domain wall states between 2D faces with oppositely gapped fourfold Dirac fermions [7,89]. By enumerating the parity eigenvalues of trivial (atomic) insulators, whose occupied bands define "elementary" band representations (EBRs) [48,91–96], it can be shown that the $\mathbb{Z}_2$ Fu-Kane criterion should be promoted to a $\mathbb{Z}_4$ index that captures both TIs and HOTIs [3,19,87–89]. Using EBRs [93], HOTI phases have been identified in systems with double band inversion (DBI) (Fig. 1), most notably in rhombohedral bismuth crystals [19].

Employing this $\mathbb{Z}_4$ index and Wilson loops [120–124], we identify the TMD [25] β- (1T'-) $MoTe_2$ [space group (SG) 11 $P2_1/m$] as a HOTI with large, gapped, arclike surface states, and explicitly show that, in the absence of SOC, it forms an NLSM with MNLs. This cements the suggestion, introduced in [125], that monopole nodal-line semimetals (MNLSMs) formed from DBI are the weak-SOC limit of HOTIs, in analogy to the earlier recognition [44] that monopole-trivial NLSMs are the weak-SOC limit

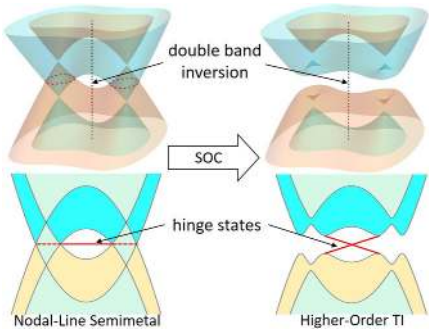

FIG. 1. When two pairs of degenerate bands with positive parity eigenvalues and two pairs with negative parity eigenvalues are inverted at a TRIM point [3,19], the occupied bands cannot be expressed as a linear combination of EBRs [48,91–96] and the $\mathbb{Z}_4$ topological index [87–90] is changed by 2. In a $\mathcal{T}$-symmetric crystal with vanishing SOC, this process may nucleate a pair of Dirac nodal lines with nontrivial monopole charge (MNLs) [46] (dashed lines in left panel). On the 1D hinges, the projections of the MNLs are spanned by nearly flat bands (an explicit model is provided in the Supplemental Material, Sec. A [97]). These hinge states represent an example of higher-order topology in a bulk-gapless system: they are the $d-2$-dimensional generalization of drumhead surface states, and are the spinless analogs of the hinge states recently predicted in spinful Dirac SMs [50,119]. When $\mathcal{I}$-symmetric SOC is introduced, the MNLSM will necessarily gap into a HOTI if all other bands are uninverted, and the flat-band hinge states will open into helical pairs spanning the bulk and surface gaps. HOTIs driven by this "double band inversion" (DBI) include bismuth [19] and, as shown in this Letter, β-$MoTe_2$ [Fig. 2(d)].

of 3D TIs. It has been shown that the noncentrosymmetric γ- (Td-) phases of XTe_2 (X = Mo, W) (SG 31 $Pmn2_1$), previously identified as type-II (tilted) Weyl (semi)metals [68–70], exhibit the same large surface states as β-$MoTe_2$. These states were previously identified as topologically trivial [70,126–137] [Fig. 4(d)], as the actual topological Fermi arcs from the Weyl points are considerably shorter [68,70,126,127,129,130]. However, using nested Wilson loops and first-principles calculations (Supplemental Material, Sec. B4 [97]), we explicitly demonstrate that γ-$MoTe_2$, which exhibits the same band ordering and surface states as β-$MoTe_2$, transitions into a nonsymmetry-indicated HOTI when its narrowly separated Weyl points are annihilated. Therefore, the large surface states in γ-XTe_2 are not trivial but, rather, are vestiges of a nearby HOTI phase, and originate from DBI, like those in β-$MoTe_2$.

TMDs are a class of readily synthesizable [25–30] layered materials. Originally highlighted for the semiconducting band gap of exfoliated monolayers [138], TMDs have recently been recognized as topological materials—quasi-2D samples of β-phase TMDs have been identified as 2D TIs [139–141], and 3D samples of γ-XTe_2 have been identified in theory [68–70] and experiment [142–144] as type-II Weyl SMs. First, we focus on $MoTe_2$, and then generalize our findings to the isostructural phases of WTe_2.

$MoTe_2$ can crystallize in two distinct structures at room temperature: the hexagonal α ($2H$) phase (SG 194 $P6_3/mmc$) and the distorted monoclinic β phase [25–27,135] [Fig. 2(a)]. When β-$MoTe_2$ is further cooled below 250 K, it transitions into the noncentrosymmetric γ phase [25,135,145]. Using first-principles calculations detailed in the Supplemental Material, Sec. B1 [97], we calculate the electronic structure of β-$MoTe_2$ with and without the effects of SOC incorporated [Figs. 2(d) and 2(b), respectively]. β-$MoTe_2$ exhibits DBI (Fig. 1) at Γ as a consequence of the β-phase lattice distortion [Fig. 2(a)]. When SOC is neglected, a $\mathcal{T}$-reversed pair of topological NLs [44,45] forms, intersecting $Y\Gamma$ in an irregular, 3D shape with a significant pucker in the k_y direction [schematically depicted in Fig. 2(c)]. The NLs [red dots in Fig. 2(b)] represent the only crossing points between the bands at E_F (taking the direct gap to lie above $N = 28$ spin-degenerate pairs of bands). As prescribed in [46,83,84], we surround each NL with a closed surface and calculate the Wilson loop (holonomy) matrix [120–124] over the lower N bands as a function of the polar momentum k_θ [Fig. 2(c) and Supplemental Material, Sec. B2 [97]]. This Wilson spectrum exhibits the characteristic winding of a MNL [46,83,84].

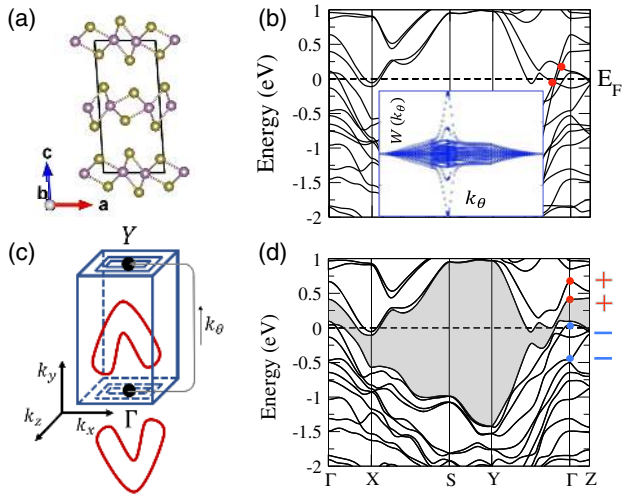

FIG. 2. (a) The monoclinic lattice of β- (1T'-) $MoTe_2$ [25] in SG 11 $P2_1/m$. (b) and (d) Bulk bands of β-$MoTe_2$ calculated without and with the effects of SOC incorporated, respectively (details provided in the Supplemental Material, Sec. B [97]). DBI occurs about the Γ point, as indicated by the parity eigenvalues in (d). (c) When SOC is neglected, a $\mathcal{T}$-reversed pair of irregularly shaped NLs forms at E_F, intersecting $Y\Gamma$ [red dots in (b)] between $k_y = \pm 0.06(2\pi/b)$ and $k_y = \pm 0.19(2\pi/b)$, where $b = 4.369$ Å is the lattice spacing along the $\vec{b}$ lattice vector [146]. We surround one of the NLs with a closed, tetragonal prism and calculate the Wilson loop around k_y-normal squares as a function of the polar momentum k_θ (exact coordinates provided in the Supplemental Material, Sec. B2 [97]); we observe $\mathbb{Z}_2$-nontrivial winding [inset panel in (b)], indicating a nontrivial monopole charge [46,83,84]. (d) When SOC is introduced, a gap near E_F develops at all crystal momenta (gray shaded region) with the $\mathbb{Z}_4$ parity index (Table I) of a HOTI [87–90].

We also explore the topology of the gapped regions between the MNLs by calculating the z-directed Wilson loop $W_1(k_x, k_y)$ [Fig. 3(a)] over the lower N bands in the absence of SOC. In BZ planes indexed by k_y away from the MNLs, $W_1(k_x, k_y)$ exhibits gaps at $\theta_1/2\pi \approx \pm 0.25$ [Figs. 3(c) and 3(d) and Supplemental Material, Sec. B3 [97]], allowing us to calculate a nested Wilson loop matrix $W_2(k_y)$ for which $\det[W_2(k_y)] = \exp(i\gamma_2)$, where γ_2 is the nested Berry phase [1–3]. In bulk-gapped k_y-indexed planes, $\det[W_2(k_y)]$ is quantized at ± 1 [Fig. 3(b)], indicating that $\gamma_2 = \pi$ (0) below (above) the MNL, implying that the Hamiltonians $\mathcal{H}_{k_y}(k_x, k_z)$ of planes in the two regions are topologically distinct. This quantization can be understood from two perspectives: the bulk and the Wilson loop. From a bulk perspective, $\mathcal{H}_{k_y}(k_x, k_z)$ is invariant under a local spinless time-reversal symmetry $\mathcal{I} \times \tilde{\mathcal{T}}$ that preserves the signs of $k_{x,z}$ and squares to $+1$. $\mathcal{H}_{k_y}(k_x, k_z)$, therefore, lies in Class AI of the Altland-Zirnbauer classification [147,148] with codimension [44,149] $D \mod 8 = 6$, implying a $\mathbb{Z}_2$ topology. This topology can be diagnosed by considering the Wilson-loop perspective. In the Supplemental Material, Sec. B3 [97], we show that $\mathcal{I} \times \tilde{\mathcal{T}}$, which acts on $W_1(k_x, k_y)$ as an antiunitary particle-hole symmetry $\tilde{\Xi}$ that preserves the signs of $k_{x,y}$ [7,122,124], enforces $\det[W_2(k_y)] = \pm 1$ when it is evaluated over any $\tilde{\Xi}$-symmetric grouping of Wilson bands

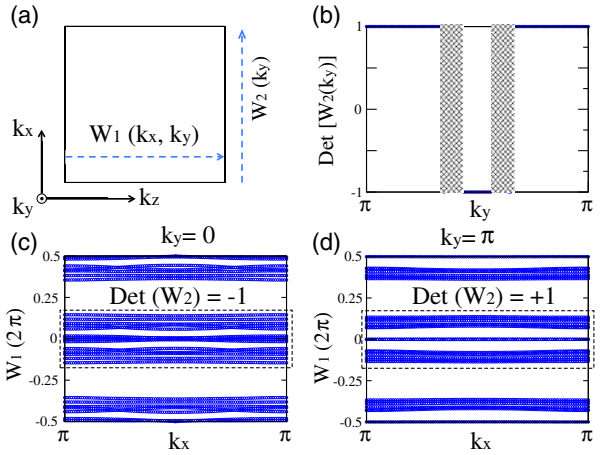

FIG. 3. (a) Bulk Wilson loops calculated for β-$MoTe_2$ from first principles in the absence of SOC (Supplemental Material, Sec. B3 [97]). At values of k_y away from the MNLs in Fig. 2, there is a large gap in the z-directed Wilson loop spectrum $W_1(k_x, k_y)$ between $\theta_1/2\pi \approx \pm 0.25$; representative examples are shown in (c) and (d) for $k_y = 0$, π, respectively. (b) The determinant of the nested Wilson matrix $W_2(k_y)$ calculated over the Wilson bands between $\theta_1 = \pm\pi/2$ [1–3,50] is quantized at ± 1 by the antiunitary symmetry $(\mathcal{I} \times \tilde{\mathcal{T}})^2 = +1$ (Supplemental Material, Sec. B3a [97]), and jumps as it passes over an MNL, indicating that k_y-indexed planes above and below the MNL are topologically distinct [1–3].

[Figs. 3(c) and 3(d)], including (but not limited to) the Wilson bands between $\theta_1/2\pi \approx \pm 0.25$ in Figs. 3(c) and 3(d). Crucially, building on [1,2,50], which employ a different definition of γ_2 reliant on fourfold rotation symmetry, the π shift in γ_2 indicates that $\mathcal{H}_{k_y}(k_x, k_z)$ above and below an MNL are equivalent to topologically distinct 2D magnetic atomic limits [50,93] (or trivialized fragile phases [11,47–51]) that differ by the presence or absence of topological corner (hinge) modes (Supplemental Material, Sec. A [97]). This implies that MNLSMs are higher-order topological SMs [50,119] with flat-band-like hinge states (Fig. 1 and Supplemental Material, Sec. A [97]). Thus, the jump in γ_2 as k_y passes through an MNL [Fig. 3(b)] represents a new example of a topological "descent relation," analogous to the jump in Berry phase as the line on which it is calculated passes through a Dirac point in 2D and an NL in 3D [44]. As in a Weyl SM [150,151], the winding of the Wilson loop evaluated on a closed surface around the MNL [Fig. 2(b)] captures the difference in topology between the gapped planes above and below it [46], which, here, is the gapless point in W_1 (which is well defined when W_1 is evaluated on a slightly distorted path that avoids the MNLs).

When SOC is introduced, β-$MoTe_2$, though remaining metallic, develops a gap at all crystal momenta [Fig. 2(d)]. Calculating the parity eigenvalues (Table I), we find that, though the Fu-Kane $\mathbb{Z}_2$ index [79,80] is trivial, the occupied bands, nevertheless, cannot be expressed as a sum of EBRs, indicating an overall nontrivial topology [93]. Specifically, while every EBR in an $\mathcal{I}$-symmetric space group exhibits Kramers pairs of parity eigenvalues [93,94] for which $\sum n_-(\vec{k}) \bmod 4 = 0$, the DBI in β-$MoTe_2$ induces an insulator with $\sum n_-(\vec{k}) \bmod 4 = 2$ (Table I). Alternatively, this defines a $\mathbb{Z}_4$ index [87–90] which is nontrivial. From both perspectives, β-$MoTe_2$ carries the parity eigenvalues of a HOTI [3,19]. Therefore, like bismuth [19,152,153], β-$MoTe_2$ is a 2D TI when viewed as a quasi-2D system [139–141], but is actually a HOTI when taken to be fully 3D.

Unlike β-$MoTe_2$, β-WTe_2, while stabilizable as a monolayer [27,141], is unstable as a bulk crystal [155]. Nevertheless, the calculated electronic structure of artificial β-WTe_2 also exhibits DBI at the Γ point [155], indicating that it would also be a HOTI if it could be stabilized. However, shortly, we will see that remnants of this HOTI phase are still observable in γ-WTe_2.

In Figs. 4(d) and 4(e), we plot the (001) surface states of β-$MoTe_2$ calculated from first-principles (Supplemental Material, Sec. B1 [97]). We observe large, arclike surface states around the projection of the Γ point [white arrows in Fig. 4(d)], as well the projections of bulk states at the

TABLE I. The number of Kramers pairs with -1 parity eigenvalues $n_-(\vec{k})$ at each TRIM point in β-$MoTe_2$ (Supplemental Material, Sec. B1 [97]). The $\mathbb{Z}_4$ index [87–90] $\sum n_-(\vec{k}) \bmod 4 = 2$. Along with the trivial weak indices [79,80,154] and the absence of fourfold and sixfold rotation symmetries [2–4,76,87,89], this indicates that β-$MoTe_2$ is a HOTI.

TRIM	Γ	X	Y	Z	S	T	U	R
$n_-(\vec{k})$	12	14	14	14	14	14	14	14

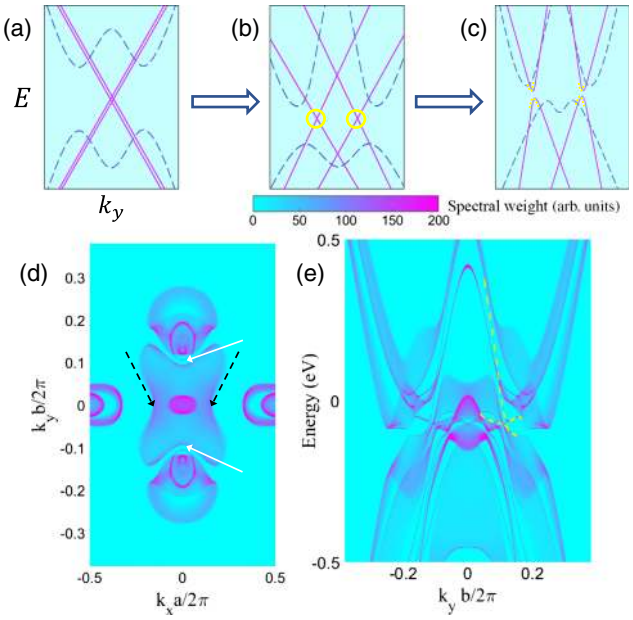

FIG. 4. (a)–(c) Schematic surface state evolution of a HOTI driven by DBI. (a) Two bulk bands inverted at the same energy (blue dashed lines) realize a fourfold surface Dirac fermion (purple lines) [19]. (b) In the absence of specific glide reflection symmetries, this fermion is unstable [7], and will split into two, twofold surface fermions, which may be stabilized by either a surface mirror [topological crystalline insulator (TCI)] [72,157], glide (hourglass TCI) [7,75], or $C_{2z} \times \mathcal{T}$ symmetry (rotation anomaly TCI) [11,76,158]. (c) In the absence of surface reflection or rotation symmetries, the twofold cones [yellow circles in (b), dashed lines in (c)] hybridize and gap, realizing the surface of a HOTI [3]. (d) Spectral weight at E_F of states on the (001) surface of β-$MoTe_2$ plotted as a function of $k_{x,y}$, and (e) along $k_x = 0$ as a function of energy (Supplemental Material, Sec. B1 [97]). Each of the two band inversions at the bulk Γ point [Fig. 2(d)] nucleates a topological twofold surface cone centered at $k_x = k_y = 0$ (purple); the cones then repel each other in energy and merge with the projections of the bulk states (b). As depicted in (c), the surface bands from these cones [white arrows in (d)] hybridize and gap [yellow dashed lines in (e)] to form a narrowly avoided crossing. In $\gamma - XTe_2$, these hybridized cones also appear as surface states [68–70,127–137], but their gap is spanned along k_x by small, topological Fermi arcs from bulk type-II Weyl points below E_F [black arrows in (d)]. In the Supplemental Material, Sec. B4 [97], we calculate the (001) surface states of γ-$MoTe_2$ gapped with symmetry-preserving distortion, and observe gapped HOTI surface states nearly identical to those in β-$MoTe_2$ [(d) and (e)].

$k_y = 0$ surface TRIM points. Crucially, we determine that the surface states are, in fact, gapped at all values of $k_{x,y}$. This can be understood by considering the symmetry and topology consequences of the bulk DBI at Γ. In the absence of SOC, each band inversion nucleates one drumhead surface state (per spin) around the surface projection of the Γ point (Supplemental Material, Sec. A [97]). In the absence of additional surface wallpaper group symmetries, such as mirror or glide [7,156], these drumhead states hybridize and gap. When SOC is reintroduced, the four hybridized drumhead states (two per spin) open into two hybridized twofold surface TI cones [Figs. 4(a)–4(c)]. Therefore, rather than being trivial Fermi arcs, the surface states of β-$MoTe_2$ are, in fact, the characteristic split and gapped fourfold Dirac-cone states of a HOTI [3,7,19]. Unlike the gapless surface states of 3D TIs [79,80], the gapped Fermi arcs only appear at low energies because of the interplay of SOC and band dispersion in β-$MoTe_2$ and, theoretically, could be moved away from E_F without changing the bulk or surface topology (Supplemental Material, Sec. A [97]).

This observation solves a longstanding mystery in γ-XTe_2. In theoretical predictions [68–70] and bulk experimental probes [142–144], both γ-$MoTe_2$ and γ-WTe_2 exhibit narrowly separated type-II Weyl points in the vicinity of doubly inverted bands. Nevertheless, as measured both directly by angle-resolved photoemission spectroscopy [127,128,130,131,136] and through quasiparticle interference in STM probes [133–135], γ-XTe_2 crystals also exhibit huge, arclike surface states that largely overwhelm possible signatures of topological Weyl Fermi arcs. Previous works determined these large surface arcs to be topologically trivial [68–70,127–135]. However, in light of our previous analysis of similar nontrivial surface states in β-$MoTe_2$, we recognize this determination to be incomplete. By explicitly calculating the surface states and bulk topology of γ-$MoTe_2$ when its Weyl points are gapped by slight distortion (Supplemental Material, Sec. B4 [97]), we, instead, discover that the large Fermi arcs in γ-XTe_2 represent the split surface Dirac cones of a nonsymmetry-indicated HOTI phase that is nearby in parameter space and driven by DBI (Fig. 4). Given the small separation of the bulk Weyl points, which is quite sensitive to experimental conditions [135,136,159,160], this HOTI phase may be accessible via symmetry-preserving distortion or strain, and may already be realized in existing samples.

In this Letter, we have demonstrated higher-order topology in both β- and γ-XTe_2. When SOC is neglected in β-$MoTe_2$, we observe a pair of MNLs at E_F. While SOC cannot be neglected in β-$MoTe_2$, other centrosymmetric materials with lighter atoms and DBI are likely to also exhibit MNLs [46]. When the effects of SOC are incorporated, β-$MoTe_2$ develops a direct gap with the parity eigenvalues of a HOTI. Though β-$MoTe_2$ is, in fact, metallic, and thus, does not host the projected hinge gap required to observe its characteristic helical hinge modes [19], it is possible that a TMD with more favorable band dispersion could be engineered by intercalation or chemical substitution. Finally, we observe that both γ-$MoTe_2$ and γ-WTe_2 exhibit the same large topological surface arcs as β-$MoTe_2$, resolving an outstanding puzzle in TMDs, and presenting a new venue for investigating nonsymmetry-indicated higher-order topology.

The authors thank Barry Bradlyn, Jennifer Cano, Yichen Hu, Fan Zhang, and Youngkuk Kim for helpful discussions. Z. W., B. J. W., and B. A. B. were supported by the Department of Energy Grant No. DE-SC0016239, the National Science Foundation EAGER Grants No. DMR 1643312 and NSF-MRSEC No. DMR-1420541, Army Research Office Grant No. ARO MURI W911NF-12-1-0461, Simons Investigator Grant No. 404513, ONR Grant No. N00014-14-1-0330, the Packard Foundation, the Schmidt Fund for Innovative Research, and a Guggenheim Fellowship from the John Simon Guggenheim Memorial Foundation. Z. W. additionally acknowledges support from the National Thousand-Young-Talents Program and the CAS Pioneer Hundred Talents Program. This work was also supported by the National Natural Science Foundation of China (Grants No. 11504117 and No. 11774317). B. Y. acknowledges support from the Willner Family Leadership Institute for the Weizmann Institute of Science, the Benoziyo Endowment Fund for the Advancement of Science, the Ruth and Herman Albert Scholars Program for New Scientists, and the European Research Council (ERC) under the European Union Horizon 2020 Research and Innovation Programme (Grant No. 815869).

Z. W. and B. J. W. contributed equally to this work.

Note added.—Recently, hinge states in β-$MoTe_2$ were also predicted in [161], but the relationship between higher-order topology in β-$MoTe_2$, MNLs, Fermi arcs in γ-XTe_2, and the experimental data were not previously established. In a revised version of [46], fragile topology was also recognized in 2D insulators with $\mathcal{I} \times \tilde{\mathcal{T}}$ symmetry. The fragile-phase corner charges introduced in this Letter were subsequently verified and further explored in [11,12,162–164], and were demonstrated in [11,12,165], along with the alternative formulation of the nested Wilson loop introduced in this Letter (Supplemental Material, Sec. B3 [97]), to be essential components of the pumping formulation of axion insulators. The flat-band-like MNL hinge states predicted in this Letter were subsequently observed in first-principles calculations of 3D graphdiyne [166]. The nested Jackiw-Rebbi formulation of fragile-phase corner charges employed in this Letter (Supplemental Material, Sec. A [97], adapted from [50]) was subsequently generalized in [164] to characterize the (anomalous) 0D boundary modes of $\mathcal{I}$-symmetric fragile phases with arbitrary dimensionality. Finally, incipient experimental signatures of hinge states in $MoTe_2$ and WTe_2 were observed in [167,168], respectively.

[1] W. A. Benalcazar, B. A. Bernevig, and T. L. Hughes, Science **357**, 61 (2017).
[2] W. A. Benalcazar, B. A. Bernevig, and T. L. Hughes, Phys. Rev. B **96**, 245115 (2017).
[3] F. Schindler, A. M. Cook, M. G. Vergniory, Z. Wang, S. S. P. Parkin, B. A. Bernevig, and T. Neupert, Sci. Adv. **4**, eaat0346 (2018).
[4] Z. Song, Z. Fang, and C. Fang, Phys. Rev. Lett. **119**, 246402 (2017).
[5] J. Langbehn, Y. Peng, L. Trifunovic, F. von Oppen, and P. W. Brouwer, Phys. Rev. Lett. **119**, 246401 (2017).
[6] L. Trifunovic and P. W. Brouwer, Phys. Rev. X **9**, 011012 (2019).
[7] B. J. Wieder, B. Bradlyn, Z. Wang, J. Cano, Y. Kim, H.-S. D. Kim, A. M. Rappe, C. L. Kane, and B. A. Bernevig, Science **361**, 246 (2018).
[8] F. Zhang, C. L. Kane, and E. J. Mele, Phys. Rev. Lett. **110**, 046404 (2013).
[9] M. Ezawa, Phys. Rev. B **97**, 155305 (2018).
[10] F. Liu and K. Wakabayashi, Phys. Rev. Lett. **118**, 076803 (2017).
[11] B. J. Wieder and B. A. Bernevig, arXiv:1810.02373.
[12] J. Ahn and B.-J. Yang, Phys. Rev. B **99**, 235125 (2019).
[13] B. J. Wieder, Y. Kim, A. M. Rappe, and C. L. Kane, Phys. Rev. Lett. **116**, 186402 (2016).
[14] B. Bradlyn, J. Cano, Z. Wang, M. G. Vergniory, C. Felser, R. J. Cava, and B. A. Bernevig, Science **353**, aaf5037 (2016).
[15] G. Chang, B. J. Wieder, F. Schindler, D. S. Sanchez, I. Belopolski, S.-M. Huang, B. Singh, D. Wu, T.-R. Chang, T. Neupert *et al.*, Nat. Mater. **17**, 978 (2018).
[16] G. Chang, S.-Y. Xu, B. J. Wieder, D. S. Sanchez, S.-M. Huang, I. Belopolski, T.-R. Chang, S. Zhang, A. Bansil, H. Lin *et al.*, Phys. Rev. Lett. **119**, 206401 (2017).
[17] P. Tang, Q. Zhou, and S.-C. Zhang, Phys. Rev. Lett. **119**, 206402 (2017).
[18] S. M. Young and B. J. Wieder, Phys. Rev. Lett. **118**, 186401 (2017).
[19] F. Schindler, Z. Wang, M. G. Vergniory, A. M. Cook, A. Murani, S. Sengupta, A. Y. Kasumov, R. Deblock, S. Jeon, I. Drozdov *et al.*, Nat. Phys. **14**, 918 (2018).
[20] N. B. M. Schröter, D. Pei, M. G. Vergniory, Y. Sun, K. Manna, F. de Juan, J. A. Krieger, V. Süss, M. Schmidt, P. Dudin *et al.*, Nat. Phys. **15**, 759 (2019).
[21] D. S. Sanchez, I. Belopolski, T. A. Cochran, X. Xu, J.-X. Yin, G. Chang, W. Xie, K. Manna, V. Süß, C.-Y. Huang *et al.*, Nature (London) **567**, 500 (2019).
[22] D. Takane, Z. Wang, S. Souma, K. Nakayama, T. Nakamura, H. Oinuma, Y. Nakata, H. Iwasawa, C. Cacho, T. Kim *et al.*, Phys. Rev. Lett. **122**, 076402 (2019).
[23] Z. Rao, H. Li, T. Zhang, S. Tian, C. Li, B. Fu, C. Tang, L. Wang, Z. Li, W. Fan *et al.*, Nature (London) **567**, 496 (2019).
[24] N. B. M. Schröter, S. Stolz, K. Manna, F. de Juan, M. G. Vergniory, J. A. Krieger1, D. Pei, P. Dudin, T. K. Kim, C. Cacho *et al.*, arXiv:1907.08723.
[25] W. G. Dawson and D. W. Bullett, J. Phys. C **20**, 6159 (1987).
[26] C. H. Naylor, W. M. Parkin, Z. Gao, J. Berry, S. Zhou, Q. Zhang, J. B. McClimon, L. Z. Tan, C. E. Kehayias, M.-Q. Zhao *et al.*, ACS Nano **11**, 8619 (2017).
[27] C. H. Naylor, W. M. Parkin, Z. Gao, H. Kang, M. Noyan, R. B. Wexler, L. Z. Tan, Y. Kim, C. E. Kehayias, F. Streller *et al.*, 2D Mater. **4**, 021008 (2017).
[28] Y. Gao, Z. Liu, D.-M. Sun, L. Huang, L.-P. Ma, L.-C. Yin, T. Ma, Z. Zhang, X.-L. Ma, L.-M. Peng *et al.*, Nat. Commun. **6**, 8569 (2015).
[29] G. Eda, T. Fujita, H. Yamaguchi, D. Voiry, M. Chen, and M. Chhowalla, ACS Nano **6**, 7311 (2012).
[30] M. N. Ali, J. Xiong, S. Flynn, J. Tao, Q. D. Gibson, L. M. Schoop, T. Liang, N. Haldolaarachchige, M. Hirschberger, N. P. Ong *et al.*, Nature (London) **514**, 205 (2014).
[31] F. Wilczek, Phys. Rev. Lett. **58**, 1799 (1987).
[32] A. M. Essin, J. E. Moore, and D. Vanderbilt, Phys. Rev. Lett. **102**, 146805 (2009).
[33] N. Varnava and D. Vanderbilt, Phys. Rev. B **98**, 245117 (2018).
[34] X.-L. Qi, T. L. Hughes, and S.-C. Zhang, Phys. Rev. B **78**, 195424 (2008).
[35] T. L. Hughes, E. Prodan, and B. A. Bernevig, Phys. Rev. B **83**, 245132 (2011).
[36] X. Chen, L. Fidkowski, and A. Vishwanath, Phys. Rev. B **89**, 165132 (2014).
[37] A. M. Turner, Y. Zhang, and A. Vishwanath, Phys. Rev. B **82**, 241102(R) (2010).
[38] L. Wu, M. Salehi, N. Koirala, J. Moon, S. Oh, and N. P. Armitage, Science **354**, 1124 (2016).
[39] S. T. Ramamurthy, Y. Wang, and T. L. Hughes, Phys. Rev. Lett. **118**, 146602 (2017).
[40] F. Schindler, S. S. Tsirkin, T. Neupert, B. A. Bernevig, and B. J. Wieder (to be published).
[41] S. Liang, S. Kushwaha, T. Gao, M. Hirschberger, J. Li, Z. Wang, K. Stolze, B. Skinner, B. A. Bernevig, R. J. Cava *et al.*, Nat. Mater. **18**, 443 (2019).
[42] B. Bradlyn (private communication).
[43] B. J. Wieder, A. Gromov, and B. Bradlyn (to be published).
[44] Y. Kim, B. J. Wieder, C. L. Kane, and A. M. Rappe, Phys. Rev. Lett. **115**, 036806 (2015).
[45] C. Fang, Y. Chen, H.-Y. Kee, and L. Fu, Phys. Rev. B **92**, 081201(R) (2015).
[46] J. Ahn, D. Kim, Y. Kim, and B.-J. Yang, Phys. Rev. Lett. **121**, 106403 (2018).
[47] H. C. Po, H. Watanabe, and A. Vishwanath, Phys. Rev. Lett. **121**, 126402 (2018).
[48] J. Cano, B. Bradlyn, Z. Wang, L. Elcoro, M. G. Vergniory, C. Felser, M. I. Aroyo, and B. A. Bernevig, Phys. Rev. Lett. **120**, 266401 (2018).
[49] J. Cano, B. Bradlyn, L. Elcoro, Z. Wang, and B. A. Bernevig (to be published).
[50] B. J. Wieder, Z. Wang, J. Cano, X. Dai, L. M. Schoop, B. Bradlyn, and B. A. Bernevig, arXiv:1908.00016.
[51] A. Bouhon, A. M. Black-Schaffer, and R.-J. Slager, arXiv:1804.09719.
[52] P. R. Wallace, Phys. Rev. **71**, 622 (1947).
[53] G. W. Semenoff, Phys. Rev. Lett. **53**, 2449 (1984).
[54] D. P. DiVincenzo and E. J. Mele, Phys. Rev. B **29**, 1685 (1984).
[55] C. L. Kane and E. J. Mele, Phys. Rev. Lett. **95**, 146802 (2005).
[56] B. A. Bernevig, T. L. Hughes, and S.-C. Zhang, Science **314**, 1757 (2006).

[57] C. L. Kane and E. J. Mele, Phys. Rev. Lett. **95**, 226801 (2005).
[58] N. P. Armitage, E. J. Mele, and A. Vishwanath, Rev. Mod. Phys. **90**, 015001 (2018).
[59] B. Yan and C. Felser, Annu. Rev. Condens. Matter Phys. **8**, 337 (2017).
[60] Z. K. Liu, B. Zhou, Y. Zhang, Z. J. Wang, H. M. Weng, D. Prabhakaran, S.-K. Mo, Z. X. Shen, Z. Fang, X. Dai *et al.*, Science **343**, 864 (2014).
[61] C.-K. Chiu and A. P. Schnyder, J. Phys. Conf. Ser. **603**, 012002 (2015).
[62] B.-J. Yang and N. Nagaosa, Nat. Commun. **5**, 4898 (2014).
[63] Z. Wang, H. Weng, Q. Wu, X. Dai, and Z. Fang, Phys. Rev. B **88**, 125427 (2013).
[64] S.-Y. Xu, C. Liu, S. K. Kushwaha, R. Sankar, J. W. Krizan, I. Belopolski, M. Neupane, G. Bian, N. Alidoust, T.-R. Chang *et al.*, Science **347**, 294 (2015).
[65] S. Borisenko, Q. Gibson, D. Evtushinsky, V. Zabolotnyy, B. Büchner, and R. J. Cava, Phys. Rev. Lett. **113**, 027603 (2014).
[66] S. M. Young, S. Zaheer, J. C. Y. Teo, C. L. Kane, E. J. Mele, and A. M. Rappe, Phys. Rev. Lett. **108**, 140405 (2012).
[67] X. Wan, A. M. Turner, A. Vishwanath, and S. Y. Savrasov, Phys. Rev. B **83**, 205101 (2011).
[68] A. A. Soluyanov, D. Gresch, Z. Wang, Q. Wu, M. Troyer, X. Dai, and B. A. Bernevig, Nature (London) **527**, 495 (2015).
[69] Z. Wang, D. Gresch, A. A. Soluyanov, W. Xie, S. Kushwaha, X. Dai, M. Troyer, R. J. Cava, and B. A. Bernevig, Phys. Rev. Lett. **117**, 056805 (2016).
[70] Y. Sun, S.-C. Wu, M. N. Ali, C. Felser, and B. Yan, Phys. Rev. B **92**, 161107(R) (2015).
[71] L. Fu, Phys. Rev. Lett. **106**, 106802 (2011).
[72] T. H. Hsieh, H. Lin, J. Liu, W. Duan, A. Bansil, and L. Fu, Nat. Commun. **3**, 982 (2012).
[73] Z. Wang and S.-C. Zhang, Phys. Rev. B **87**, 161107(R) (2013).
[74] S. M. Young and C. L. Kane, Phys. Rev. Lett. **115**, 126803 (2015).
[75] Z. Wang, A. Alexandradinata, R. J. Cava, and B. A. Bernevig, Nature (London) **532**, 189 (2016).
[76] C. Fang and L. Fu, arXiv:1709.01929.
[77] R. Yu, H. Weng, Z. Fang, X. Dai, and X. Hu, Phys. Rev. Lett. **115**, 036807 (2015).
[78] Y.-H. Chan, C.-K. Chiu, M. Y. Chou, and A. P. Schnyder, Phys. Rev. B **93**, 205132 (2016).
[79] L. Fu, C. L. Kane, and E. J. Mele, Phys. Rev. Lett. **98**, 106803 (2007).
[80] L. Fu and C. L. Kane, Phys. Rev. B **76**, 045302 (2007).
[81] L. S. Xie, L. M. Schoop, E. M. Seibel, Q. D. Gibson, W. Xie, and R. J. Cava, APL Mater. **3**, 083602 (2015).
[82] H. Weng, Y. Liang, Q. Xu, R. Yu, Z. Fang, X. Dai, and Y. Kawazoe, Phys. Rev. B **92**, 045108 (2015).
[83] A. Bouhon and A. M. Black-Schaffer, arXiv:1710.04871.
[84] T. Bzdušek and M. Sigrist, Phys. Rev. B **96**, 155105 (2017).
[85] K. Li, C. Li, J. Hu, Y. Li, and C. Fang, Phys. Rev. Lett. **119**, 247202 (2017).
[86] G. Li, Y. Li, H. Liu, Y. Guo, Y. Li, and D. Zhu, Chem. Commun. **46**, 3256 (2010).
[87] Z. Song, T. Zhang, Z. Fang, and C. Fang, Nat. Commun. **9**, 3530 (2018).
[88] H. C. Po, A. Vishwanath, and H. Watanabe, Nat. Commun. **8**, 50 (2017).
[89] E. Khalaf, H. C. Po, A. Vishwanath, and H. Watanabe, Phys. Rev. X **8**, 031070 (2018).
[90] E. Khalaf, Phys. Rev. B **97**, 205136 (2018).
[91] J. Zak, Phys. Rev. B **23**, 2824 (1981).
[92] J. Zak, Phys. Rev. B **26**, 3010 (1982).
[93] B. Bradlyn, L. Elcoro, J. Cano, M. G. Vergniory, Z. Wang, C. Felser, M. I. Aroyo, and B. A. Bernevig, Nature (London) **547**, 298 (2017).
[94] L. Elcoro, B. Bradlyn, Z. Wang, M. G. Vergniory, J. Cano, C. Felser, B. A. Bernevig, D. Orobengoa, G. de la Flor, and M. I. Aroyo, J. Appl. Crystallogr. **50**, 1457 (2017).
[95] M. G. Vergniory, L. Elcoro, Z. Wang, J. Cano, C. Felser, M. I. Aroyo, B. A. Bernevig, and B. Bradlyn, Phys. Rev. E **96**, 023310 (2017).
[96] J. Cano, B. Bradlyn, Z. Wang, L. Elcoro, M. G. Vergniory, C. Felser, M. I. Aroyo, and B. A. Bernevig, Phys. Rev. B **97**, 035139 (2018).
[97] See Supplemental Material at http://link.aps.org/supplemental/10.1103/PhysRevLett.123.186401 for tight-binding models demonstrating the presence of hinge states in MNLSMs, first-principles calculation details, a proof of the quantization of the nested Berry phase in the presence of $\mathcal{I}\times\mathcal{T}$ symmetry, confirmation of nonsymmetry-indicated higher-order topology in gapped noncentrosymmetric (γ phase) $MoTe_2$ through nested Wilson loop and surface state calculations, which includes Refs. [98–118].
[98] W. Setyawan and S. Curtarolo, Comput. Mater. Sci. **49**, 299 (2010).
[99] Python tight binding open-source package, http://physics.rutgers.edu/pythtb/.
[100] R. Jackiw and C. Rebbi, Phys. Rev. D **13**, 3398 (1976).
[101] M. Pretko, Phys. Rev. B **96**, 035119 (2017).
[102] D. B. Litvin, *Magnetic Group Tables* (International Union of Crystallography, 2013), https://www.iucr.org/publications/iucr/magnetic-group-tables.
[103] A. H. Castro Neto, F. Guinea, N. M. R. Peres, K. S. Novoselov, and A. K. Geim, Rev. Mod. Phys. **81**, 109 (2009).
[104] M. Fujita, K. Wakabayashi, K. Nakada, and K. Kusakabe, J. Phys. Soc. Jpn. **65**, 1920 (1996).
[105] K. Nakada, M. Fujita, G. Dresselhaus, and M. S. Dresselhaus, Phys. Rev. B **54**, 17954 (1996).
[106] P. Ruffieux, S. Wang, B. Yang, C. Sánchez-Sánchez, J. Liu, T. Dienel, L. Talirz, P. Shinde, C. A. Pignedoli, D. Passerone *et al.*, Nature (London) **531**, 489 (2016).
[107] F. Zhang, Synth. Met. **210**, 9 (2015),
[108] F. D. M. Haldane, Phys. Rev. Lett. **61**, 2015 (1988).
[109] P. E. Blöchl, Phys. Rev. B **50**, 17953 (1994).
[110] G. Kresse and D. Joubert, Phys. Rev. B **59**, 1758 (1999).
[111] G. Kresse and J. Hafner, Phys. Rev. B **47**, 558 (1993).
[112] G. Kresse and J. Furthmüller, Comput. Mater. Sci. **6**, 15 (1996).

[113] J. P. Perdew, K. Burke, and M. Ernzerhof, Phys. Rev. Lett. **77**, 3865 (1996).

[114] *Inorganic Crystal Structure Database (ICSD)* (Fachinformationszentrum Karlsruhe, Karlsruhe, Germany, 2015), https://icsd.products.fiz-karlsruhe.de/en; F. H. Allen, G. Bergerhoff, and R. Sievers, *Crystallographic Databases* (International Union of Crystallography, Chester, UK, 1987).

[115] I. Souza, N. Marzari, and D. Vanderbilt, Phys. Rev. B **65**, 035109 (2001).

[116] A. M. Ilia, P.-M. J. Manuel, C. Cesar, K. Eli, I. Svetoslav, M. Gotzon, K. Asen, and W. Hans, Z. Kristallogr.—Cryst. Mater. **221**, 15 (2006).

[117] C. J. Bradley and A. P. Cracknell, *The Mathematical Theory of Symmetry in Solids* (Clarendon Press, Oxford, 1972).

[118] O. Vafek and A. Vishwanath, Annu. Rev. Condens. Matter Phys. **5**, 83 (2014).

[119] M. Lin and T. L. Hughes, Phys. Rev. B **98**, 241103(R) (2018).

[120] L. Fidkowski, T. S. Jackson, and I. Klich, Phys. Rev. Lett. **107**, 036601 (2011).

[121] R. Yu, X. L. Qi, A. Bernevig, Z. Fang, and X. Dai, Phys. Rev. B **84**, 075119 (2011).

[122] A. Alexandradinata, X. Dai, and B. A. Bernevig, Phys. Rev. B **89**, 155114 (2014).

[123] A. Alexandradinata and B. A. Bernevig, Phys. Rev. B **93**, 205104 (2016).

[124] A. Alexandradinata, Z. Wang, and B. A. Bernevig, Phys. Rev. X **6**, 021008 (2016).

[125] Z. Song, T. Zhang, and C. Fang, Phys. Rev. X **8**, 031069 (2018).

[126] A. Tamai, Q. S. Wu, I. Cucchi, F. Y. Bruno, S. Riccò, T. K. Kim, M. Hoesch, C. Barreteau, E. Giannini, C. Besnard *et al.*, Phys. Rev. X **6**, 031021 (2016).

[127] F. Y. Bruno, A. Tamai, Q. S. Wu, I. Cucchi, C. Barreteau, A. de la Torre, S. McKeown Walker, S. Riccò, Z. Wang, T. K. Kim *et al.*, Phys. Rev. B **94**, 121112(R) (2016).

[128] C. Wang, Y. Zhang, J. Huang, S. Nie, G. Liu, A. Liang, Y. Zhang, B. Shen, J. Liu, C. Hu *et al.*, Phys. Rev. B **94**, 241119(R) (2016).

[129] I. Belopolski, S.-Y. Xu, Y. Ishida, X. Pan, P. Yu, D. S. Sanchez, H. Zheng, M. Neupane, N. Alidoust, G. Chang *et al.*, Phys. Rev. B **94**, 085127 (2016).

[130] J. Jiang, Z. K. Liu, Y. Sun, H. F. Yang, C. R. Rajamathi, Y. P. Qi, L. X. Yang, C. Chen, H. Peng, C.-C. Hwang *et al.*, Nat. Commun. **8**, 13973 (2017).

[131] A. Liang, J. Huang, S. Nie, Y. Ding, Q. Gao, C. Hu, S. He, Y. Zhang, C. Wang, B. Shen *et al.*, arXiv:1604.01706.

[132] K. Deng, G. Wan, P. Deng, K. Zhang, S. Ding, E. Wang, M. Yan, H. Huang, H. Zhang, Z. Xu *et al.*, Nat. Phys. **12**, 1105 (2016).

[133] K. Kawahara, Z. Ni, R. Arafune, T. Shirasawa, C.-L. Lin, E. Minamitani, S. Watanabe, M. Kawai, and N. Takagi, Appl. Phys. Express **10**, 045702 (2017).

[134] Y. Yuan, X. Yang, L. Peng, Z.-J. Wang, J. Li, C.-J. Yi, J.-J. Xian, Y.-G. Shi, and Y.-S. Fu, Phys. Rev. B **97**, 165435 (2018).

[135] A. Notis Berger, E. Andrade, A. Kerelsky, D. Edelberg, J. Li, Z. Wang, L. Zhang, J. Kim, N. Zaki, J. Avila *et al.*, arXiv:1712.06712.

[136] Y. Wu, D. Mou, N. H. Jo, K. Sun, L. Huang, S. L. Bud'ko, P. C. Canfield, and A. Kaminski, Phys. Rev. B **94**, 121113(R) (2016).

[137] L. Huang, T. M. McCormick, M. Ochi, Z. Zhao, M.-T. Suzuki, R. Arita, Y. Wu, D. Mou, H. Cao, J. Yan *et al.*, Nat. Mater. **15**, 1155 (2016).

[138] B. Radisavljevic, A. Radenovic, J. Brivio, V. Giacometti, and A. Kis, Nat. Nanotechnol. **6**, 147 (2011).

[139] X. Qian, J. Liu, L. Fu, and J. Li, Science **346**, 1344 (2014).

[140] D.-H. Choe, H.-J. Sung, and K. J. Chang, Phys. Rev. B **93**, 125109 (2016).

[141] S. Tang, C. Zhang, D. Wong, Z. Pedramrazi, H.-Z. Tsai, C. Jia, B. Moritz, M. Claassen, H. Ryu, S. Kahn *et al.*, Nat. Phys. **13**, 683 (2017).

[142] D. Rhodes, R. Schönemann, N. Aryal, Q. Zhou, Q. R. Zhang, E. Kampert, Y.-C. Chiu, Y. Lai, Y. Shimura, G. T. McCandless *et al.*, Phys. Rev. B **96**, 165134 (2017).

[143] D. Di Sante, P. K. Das, C. Bigi, Z. Ergönenc, N. Gürtler, J. A. Krieger, T. Schmitt, M. N. Ali, G. Rossi, R. Thomale *et al.*, Phys. Rev. Lett. **119**, 026403 (2017).

[144] Y. Wu, N. H. Jo, D. Mou, L. Huang, S. L. Bud'ko, P. C. Canfield, and A. Kaminski, Phys. Rev. B **95**, 195138 (2017).

[145] X.-J. Yan, Y.-Y. Lv, L. Li, X. Li, S.-H. Yao, Y.-B. Chen, X.-P. Liu, H. Lu, M.-H. Lu, and Y.-F. Chen, npj Quantum Mater. **2**, 31 (2017).

[146] B. E. Brown, Acta Crystallogr. **20**, 268 (1966).

[147] A. Altland and M. R. Zirnbauer, Phys. Rev. B **55**, 1142 (1997).

[148] A. Kitaev, AIP Conf. Proc. **1134**, 22 (2009).

[149] J. C. Y. Teo and C. L. Kane, Phys. Rev. B **82**, 115120 (2010).

[150] L. Alvarez-Gaumé', S. Della Pietra, and G. Moore, Ann. Phys. (N.Y.) **163**, 288 (1985).

[151] H. B. Nielsen and M. Ninomiya, Nucl. Phys. **B185**, 20 (1981).

[152] S. Murakami, Phys. Rev. Lett. **97**, 236805 (2006).

[153] I. K. Drozdov, A. Alexandradinata, S. Jeon, S. Nadj-Perge, H. Ji, R. J. Cava, B. Andrei Bernevig, and A. Yazdani, Nat. Phys. **10**, 664 (2014).

[154] Z. Ringel, Y. E. Kraus, and A. Stern, Phys. Rev. B **86**, 045102 (2012).

[155] H.-J. Kim, S.-H. Kang, I. Hamada, and Y.-W. Son, Phys. Rev. B **95**, 180101(R) (2017).

[156] B. J. Wieder and C. L. Kane, Phys. Rev. B **94**, 155108 (2016).

[157] J. C. Y. Teo, L. Fu, and C. L. Kane, Phys. Rev. B **78**, 045426 (2008).

[158] C. Fang and L. Fu, Phys. Rev. B **91**, 161105(R) (2015).

[159] I. Pletikosić, M. N. Ali, A. V. Fedorov, R. J. Cava, and T. Valla, Phys. Rev. Lett. **113**, 216601 (2014).

[160] Y. Wu, N. H. Jo, M. Ochi, L. Huang, D. Mou, S. L. Bud'ko, P. C. Canfield, N. Trivedi, R. Arita, and A. Kaminski, Phys. Rev. Lett. **115**, 166602 (2015).

[161] F. Tang, H. C. Po, A. Vishwanath, and X. Wan, Nat. Phys. **15**, 470 (2019).

[162] J. Ahn, S. Park, and B.-J. Yang, Phys. Rev. X **9**, 021013 (2019).
[163] W. A. Benalcazar, T. Li, and T. L. Hughes, Phys. Rev. B **99**, 245151 (2019).
[164] Y. Hwang, J. Ahn, and B.-J. Yang, arXiv:1905.08128.
[165] E. Lee, A. Furusaki, and B.-J. Yang, arXiv:1903.02737.
[166] E. Lee, R. Kim, J. Ahn, and B.-J. Yang, arXiv:1904.11452.
[167] F.-T. Huang, S. J. Lim, S. Singh, J. Kim, L. Zhang, J.-W. Kim, M.-W. Chu, K. M. Rabe, D. Vanderbilt, and S.-W. Cheong, arXiv:1908.03082.
[168] Y.-B. Choi, Y. Xie, C.-Z. Chen, J.-H. Park, S.-B. Song, J. Yoon, B. J. Kim, T. Taniguchi, K. Watanabe, H.-J. Lee *et al.*, arXiv:1909.02537.